Nonlinear plate equation analysis for the design of large stroke deformable mirror

Oscar A. Azucena, Bautista Fernandez, Joel A. Kubby
University of California, Santa Cruz, 1156 High St., Santa Cruz, CA, USA 95064

ABSTRACT

Adaptive Optics (AO) improves the quality of astronomical imaging systems by using real time measurement of the turbulent medium in the optical path. The measurements are then taken and applied to a deformable mirror (DM) that is in the conjugate position of the aberrations in the optical path. The quality of the reconstructed wavefront directly affects the images obtained. One of the limiting factors in current DM technology is the amount of stroke available to correct the wavefront distortions which can be as high as 20 microns of optical path difference. We have developed a simulation analysis using Galerkin's method to solve the nonlinear plate equation. The analysis uses a set of orthogonal equations that satisfied the boundary condition to solve for the linear deformation on the mirror surface. This deformation is used to iteratively converge to the final solution by applying the nonlinear plate equation and the nonlinear actuator forces. This simulation was used to design a microelectromechanical DM with 10 μm of stroke.

Keywords: nonlinear plate equation, MEMS DM, adaptive optics, parallel plate actuators

1. INTRODUCTION

Adaptive Optics (AO) improves the quality of astronomical imaging systems by using real time measurement of the turbulent medium in the optical path. The measurements are then taken and applied to a Deformable Mirror (DM) that is in the conjugate position of the aberrations in the optical path. The quality of the reconstructed wavefront directly affects the images obtained. One of the limiting factors in current DM technology is the amount of stroke available to correct the wavefront distortions which can be as high as 20 microns of optical path difference. A simulation analysis using Galerkin's method to solve the nonlinear plate equation has been developed. The analysis uses a set of orthogonal equations that satisfied the boundary condition to solve for the nonlinear deformation on the mirror surface. This deformation is used to iteratively converge to the final solution by applying the nonlinear plate equation and the nonlinear actuator forces. This simulation was used to design a Micro-Electro-Mechanical Systems (MEMS) DM with 10 μm of stroke.

1.1 DM requirements and current DM technology

Hubin et. al [1] highlighted the requirements for the next generation of Extremely Large Telescopes (ELT). One of the requirements is the need for large arrays, on the order of 10,000 degrees of freedom, although this is highly dependent on the telescope size. MEMS fabrication is ideal for this since micrometer size features can be made with high aspect ratios. A 1000 actuator DM is currently available from Boston Micromachines Corporation but its stroke is only 1.5 microns [2]. Another requirement is that the DM must operate faster than the coherence time which depends on the location, time of day and weather status. The bandwidth requirement for the next generation of deformable mirrors is estimated at 1 KHz [1]. This is not really a problem for MEMS since their small size allows for much higher bandwidth. Iris AO has developed a segmented DM with a response of 150 microseconds (6.6 KHz) but the bandwidth is much smaller since the device has a small oscillation that limits their current bandwidth to approximately 2 KHz [3]. While the stroke requirement for an ELT DM is 10 μm, currently the largest stroke commercially available for a continuous membrane DM is 6μm [1]. Segmented DM's have achieved 12 microns of stroke, but they in turn produce a lot of diffraction from the segmentation, which renders them unusable in some applications. MEMS are ideal for their high repeatability; current MEMS DM have achieved good repeatability but at the cost of some of its dynamic stroke. This process has also achieved very good surface flatness but the dynamic stroke has been reduced even more. Evans et. al [4] performed a

MEMS Adaptive Optics II, edited by Scot S. Olivier, Thomas G. Bifano, Joel A. Kubby,
Proc. of SPIE Vol. 6888, 68880Q, (2008) · 0277-786X/08/$18 · doi: 10.1117/12.766873

flattening procedure on a Boston Micromachines DM. The RMS wavefront error was 148 nm before the flattening, and less than 1 nm after flattening. In this process 14% percent of the total stroke (1 μm) was lost due to flattening.

1.2 Fabrication process

The MEMS DM will be fabricated using a LIGA (Lithographie Galvanoformung Abformung) like process from HT Micro [5]. This process allows for the use of a wide variety of materials: Gold, Copper, Nickel and various ceramic substrates. The use of this high-aspect ratio processes enables very precise parts to be fabricated without the need for new process development. In the first step of the development of the MEMS DM using the HT fabrication process, electrostatic parallel plate actuators were fabricated using gold. Fernandez et. al [6] showed that a third order polynomial with respect to the actuator deflection z was proportional to the square of the voltage, $V^2 \alpha (z*(g-z)^2)$, where g is the gap. The latest results also showed that even if the actuator is slightly warped the results are the same, except that the gap should be changed to the average distance between the two parallel plates. The electrostatic parallel plate actuators will be discussed more in the next section. The final step of the fabrication process is the attachment of an optical quality gold mirror to an array of actuators. The mirror will be bonded to the actuators via posts that will be connected to the center of each actuator. The mirror will be deposited on an optical flat to reduce the amount of surface roughness. In order to reduce the amount of time and effort in fabricating the mirror surface a simulation is required in order to gain an appreciation for parameters of the membrane.

2. ACTUATOR MODEL AND NONLINEAR PLATE EQUATION

In order to simulate a MEMS DM we must account for all the forces acting on the membrane. Fig. 1 shows a cross-section of the MEMS DM. From top to bottom we see the mirror layer connected to the top of the actuator via a post. The top of the actuator is also called the spring layer since this layer will control the spring thickness for the actuator array. The spring layer is fastened to the substrate through the anchors. The electrode layer provides the second conductor of the parallel plate actuator. As we had mentioned earlier, the mirror layer will be grown on an optical flat. This will help reduce the surface roughness. The mirror layer will then be thermo-compression bonded to the posts. The simulation will give an estimate for the thickness of the mirror layer as well as the spring layer.

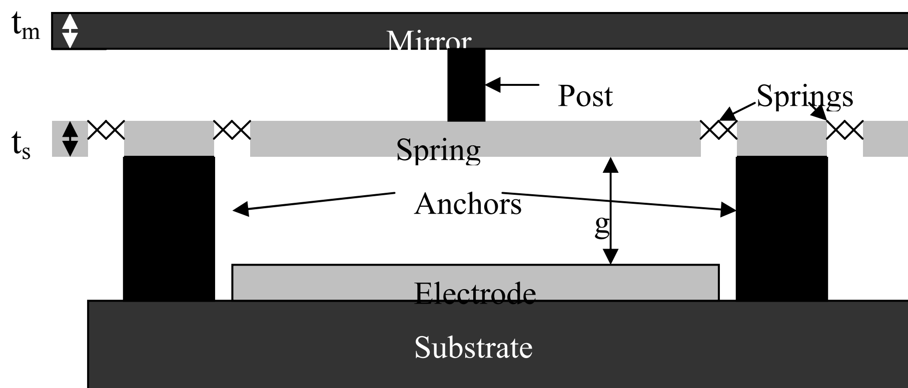

Fig 1. Cross-sectional rendering of MEMS DM that includes: Mirror Layer, Spring Layer, Electrode, Anchors and connecting post. The thickness of the mirror layer and the spring layer are two important parameters that will determine the pull-in characteristics.

2.1 Actuator model

The main force driving the MEMS DM is the electrostatic force that comes from the parallel plate actuators. Fig. 2 outlines the main features of our parallel plate actuator. The springs are evenly distributed around the four edges of the top conductor to provide better stability. Other designs have also been investigated where the springs were connected at the four corners instead of the center of each edge and circular and hexagonal plates with different spring configurations. The springs are kept in position through the anchors which are connected to the substrate. Underneath the top plate is the

bottom conductor. When a potential difference V is applied between the two plates a force is develop as the two conductors accumulate opposite charges at the surface. This force from opposite charges pulls the top plate down until the force of the springs and the mirror surface both balance the electrostatic force. The force is applied to the mirror surface through the posts, which can be considered a point contact. Previous tests on the springs showed that the springs are linear and their force can be well modeled by Hook's law:

$$F_s = -k * w \tag{1}$$

Where w is the deflection at the edges of the plate and k is the total spring constant. The main reason for a linear spring is that there is little or no stretching of the springs and the opposing force comes from longitudinal strain under pure bending.

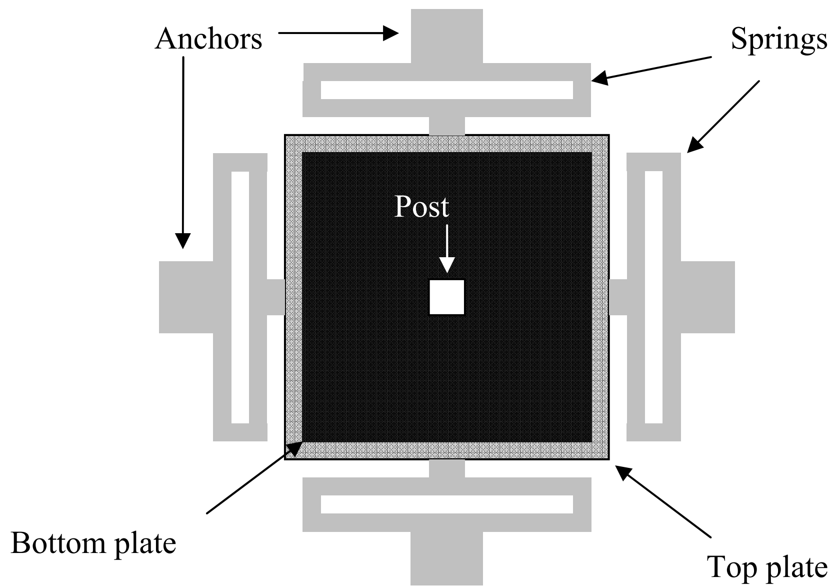

Fig 2. Top view of the parallel plate actuator. The springs were evenly distributed to provide the best stability. The anchors are designed to support two springs (one on each side). The post is also shown (not drawn to scale). Both the bottom and top plates are shown but in reality the bottom plate is fixed to the substrate.

The electrostatic force can be modeled by the following equation:

$$F_e = \frac{1}{2}\frac{\varepsilon A}{(g - w)^2}V^2 \tag{2}$$

Where ε is the permittivity of the media, A is area of the top plate (or bottom plate), g is the gap between the plates, and V is the applied voltage. F_e is a nonlinear function of g-w, which can be approximated as the average height of the actuator as long as the top plate stays relatively flat. Lab measurements have shown that even with a 1 μm dip at the center of the actuator equation 2 still holds.

Analysis of the force equilibrium using only equations 1 and 2 shows that:

$$V^2 = \frac{2}{\varepsilon A} k * w * (g - w)^2 \tag{3}$$

A more detailed analysis shows that this equation will only be true down to 2/3 of the gap (*w=g/3*). At this point the mechanical force can barely hold the plate due to the electrostatic force and at any point after that the electrical force will be greater leading to a pull-in of the plate. From this we can find what the pull-in voltage is by inserting the *g/3* limit and solving equation 3:

$$V_{pull-in} = \sqrt{\frac{8kg^3}{27\varepsilon A}} \tag{4}$$

Note that equation 4 only takes the electrical force and the mechanical force from the springs into consideration. To be more precise about the pull-in characteristics for the MEMS DM we must also include the mechanical force from the mirror layer. As was previously mentioned for a linear spring only 1/3 of the gap can be used for mechanical stroke. This corresponds to the 10 µm of mechanical stroke that is needed, which leads to a 30 µm gap. From equation 4 we also see that reducing the spring constant decreases the pull-in voltage. From fig. 2 we can deduce that the springs are a set of fixed-guided beams. Adding up the total number of springs and using the spring constant for a fixed-guided beam leads to the following equation:

$$k = 4k_{f-g} = 4\frac{Ew_p t^3}{L^3} \tag{5}$$

Where E is the Modulus of elasticity (74-78 GPa for gold), and w_p, t, and L are the width, thickness, and length of the spring respectively. For stability purposes we will set the width of the springs to be at least twice that of the mirror layer, which will also help in minimizing the deformation of the top plate. To reduce the spring constant as much as possible we will also maximize the length of the springs. The pull in voltage is inversely proportional to the square root of the plate area A, and in order to decrease the pull-in voltage we must also maximize the plate area. Table 1 shows the initial design values for the set of parameters discussed so far.

Table 1: MEMS DM Initial design parameters

Pitch	(distance between two posts)	1000µm
g	(gap)	30 µm
A	(plate area)	800µm*800µm
w_p	(plate width)	20µm
t	(spring layer thickness)	5µm
L	(spring length)	365µm
k	(total spring constant)	15N/m
$V_{pull-in}$	(pull-in voltage)	140V

2.2 Deformable mirror model

The deformable mirror can be well modeled by the plate equation [7]:

$$D\nabla^2\nabla^2 w(x,y) = p_z(x,y) \tag{6}$$

Where w is the deformation at the point (x,y), and p_z is the pressure at that same point. The flexural rigidity D depends on the modulus of elasticity E and Poisson's ratio v as follows:

$$D = \frac{Eh^3}{12(1-v^2)} \tag{7}$$

Where h is the thickness of the deformable mirror. D has a very strong dependence on its thickness just as the spring constant k does. Using Navier's method the plate equation can be transformed into a set of algebraic equations [7]. For a mirror with lengths a and b in the x and y directions, respectively, the sets of algebraic equations just mentioned only

applies to the boundary conditions shown in table 2. Note that the orthogonal set of functions that satisfied these boundary conditions are sinusoidal with period equal to the size of the mirror surface. The solution for the deflection *w* can be obtained by using equation 8:

$$w(x,y)=\sum_{m=1}^{M}\sum_{n=1}^{N}W_{mn}\sin\frac{m\pi x}{a}\sin\frac{n\pi y}{b} \tag{8}$$

Equation 8 only uses a finite subset of the infinite set which is needed to represent *w*. While Navier's method can only be applied to a linear system, (one where the loading function p_z is also linear) the set of orthogonal solutions still can be used if they are applied to more a robust method such as Galerkin's method.

Table 2: Boundary conditions for Navier's method.

$$(w)_{x=0,x=a}=(w)_{y=o,y=b}=0$$

$$(m_x)_{x=0,x=a}=-D\left(\frac{\partial^2 w}{\partial x^2}+\nu\frac{\partial^2 w}{\partial y^2}\right)=0$$

$$(m_y)_{y=o,y=b}=-D\left(\frac{\partial^2 w}{\partial y^2}+\nu\frac{\partial^2 w}{\partial x^2}\right)=0$$

Galerkin's method can be applied to a diverse set of problems which include large deflection theory of plates. Galerkin's method can be used to reduce a set of differential equations into a set of definite integrals of simplified functions [7]. Using equation 6 and Galerkin's method the solution to the plate equation is reduced to solving a set of the following equation:

$$\iint_A \left[D\nabla^2\nabla^2 w(x,y)-p_z(x,y)\right]\sin\frac{m\pi x}{a}\sin\frac{n\pi y}{b}\,dxdy=0 \tag{9}$$

Equation 9 must be applied to each set of index *m* and *n* as describe in equation 8. Note that equation 9 is a generalization of the virtual work principle. Using the basis function given in equation 8 we can further reduce equation 9 as follows:

$$\begin{aligned}
&\iint_A \left[D\sum_{i=1}^{M}\sum_{j=1}^{N}\nabla^2\nabla^2\left(W_{ij}\sin\frac{i\pi x}{a}\sin\frac{j\pi y}{b}\right)-p_z(x,y)\right]\sin\frac{m\pi x}{a}\sin\frac{m\pi y}{b}\,dxdy=\\
&\iint_A \left[D\sum_{i=1}^{M}\sum_{j=1}^{N}W_{ij}\left(\left(\frac{i\pi}{a}\right)^2+\left(\frac{j\pi}{b}\right)^2\right)^2\left(\sin\frac{i\pi x}{a}\sin\frac{j\pi y}{b}\right)-p_z(x,y)\right]\sin\frac{n\pi x}{a}\sin\frac{m\pi y}{b}\,dxdy\\
&DW_{mn}\left(\left(\frac{n\pi}{a}\right)^2+\left(\frac{m\pi}{b}\right)^2\right)^2\frac{ab}{4}-\iint_A p_z(x,y)\sin\frac{n\pi x}{a}\sin\frac{m\pi y}{b}\,dxdy=0
\end{aligned} \tag{10}$$

Using the results of equation 10 the solution of the plate equation to a given load p_z can be written in matrix form:

$$\begin{bmatrix} \left(\left(\frac{1}{a}\right)^2+\left(\frac{1}{b}\right)^2\right)^2 & . & . & . \\ . & . & . & . \\ . & . & . & . \\ . & . & . & \left(\left(\frac{M}{a}\right)^2+\left(\frac{N}{b}\right)^2\right)^2 \end{bmatrix} [W] = \begin{bmatrix} \frac{4}{Dab\pi^4}\iint_A p_z(x,y)\sin\frac{\pi x}{a}\sin\frac{\pi y}{b}dxdy \\ . \\ . \\ \frac{4}{Dab\pi^4}\iint_A p_z(x,y)\sin\frac{M\pi x}{a}\sin\frac{N\pi y}{b}dxdy \end{bmatrix} \tag{11}$$

In the case where $M=N$ the left hand side is a main diagonal matrix of size $M*M$. As we had previously mentioned the electrostatic force and the mechanical force from the actuators are coupled to the mirror via the post which can be well modeled by a point load:

$$p_z(x,y) = \sum_{c=1}^{R}\left(-kw_c + \frac{1}{2}\frac{\varepsilon A}{(g-w_c)^2}V_c^{\,2}\right)\delta(x-x_c, y-y_c) \tag{12}$$

Where R is the total number of actuators, V_c is the voltage applied at actuator c, and w_c is the deflection at the post at actuator c. Combining equation 11 and 12 the solution for the plate equation can be reduced to:

$$\left[\left(\left(\frac{m}{a}\right)^2+\left(\frac{n}{b}\right)^2\right)^2\right][W] = \begin{bmatrix} \frac{4}{Dab\pi^4}\sum_{c=1}^{R}\left(-kw_c+\frac{1}{2}\frac{\varepsilon A}{(g-w_c)^2}V_c^{\,2}\right)\sin\frac{\pi x_c}{a}\sin\frac{\pi y_c}{b} \\ . \\ . \\ \frac{4}{Dab\pi^4}\sum_{c=1}^{R}\left(-kw_c+\frac{1}{2}\frac{\varepsilon A}{(g-w_c)^2}V_c^{\,2}\right)\sin\frac{M\pi x_c}{a}\sin\frac{N\pi y_c}{b} \end{bmatrix} \tag{13}$$

Note that the deflection w_c is equal to deflection w at the point of contact (x_c,y_c). Using this information with equation 8 we can further reduce each row to:

$$\left(\left(\frac{m}{a}\right)^2+\left(\frac{n}{b}\right)^2\right)^2 W_{mn} + \frac{4k}{Dab\pi^4}\sum_{c=1}^{R}\left[\sum_{i=1}^{M}\sum_{j=1}^{N}W_{ij}\sin\frac{i\pi x_c}{a}\sin\frac{j\pi y_c}{b}\right]\sin\frac{m\pi x_c}{a}\sin\frac{n\pi y_c}{b} = \frac{4}{Dab\pi^4}\sum_{c=1}^{R}\frac{1}{2}\frac{\varepsilon A}{(g-w(x_c,y_c))^2}V_c^{\,2}\sin\frac{m\pi x_c}{a}\sin\frac{n\pi y_c}{b} \tag{14}$$

The equation above can be put into matrix form, even though the matrix is not main diagonal, its size remains $M*M$. To solve the equation above we can start by taking an initial deflection w (a good estimate for w is the average deflection for all parallel plate actuators without the mirror) then plugging it into the right hand side and solving for the new deflection. This process can be repeated until the desired relative error is achieved.

2.3 Nonlinear plate equation

If the mirror surface is deflected more than its thickness ($w_{max}>h$) vertical deflections are accompanied by stretching of the mirror surface. This stretching is a very nonlinear process which causes the mirror layer to increase its load carrying capabilities thus leading to a much higher pull-in voltage. The stretching of the mirror surface also allows for more of the gap to be use as stroke. To include this nonlinear stretching of the membrane into our model the plate equation must modified as [7]:

$$D\nabla^2\nabla^2 w(x,y) = p_z(x,y) + h\left[\frac{\partial^2 w}{\partial x^2}\left(\frac{\partial^2\Phi}{\partial y^2} + \sigma_x\right) + \frac{\partial^2 w}{\partial y^2}\left(\frac{\partial^2\Phi}{\partial x^2} + \sigma_y\right) - 2\frac{\partial^2 w}{\partial x\partial y}\left(\frac{\partial^2\Phi}{\partial x\partial y} + \sigma_{xy}\right)\right] \quad (15)$$

Where $\sigma_{x,y,xy}$ is the stress in the *x, y, xy* direction and Φ is an Airy-type stress function which can be obtained by using equation 16:

$$\nabla^2\nabla^2\Phi(x,y) = -\frac{E}{2}\left[\frac{\partial^2 w}{\partial x^2}\frac{\partial^2 w}{\partial y^2} + \frac{\partial^2 w}{\partial y^2}\frac{\partial^2 w}{\partial x^2} - 2\frac{\partial^2 w}{\partial x\partial y}\frac{\partial^2 w}{\partial x\partial y}\right] \quad (16)$$

Equations 15 and 16 are a set of nonlinear partial differential equations that must be solved simultaneously. Note that in equation 15 σ is a constant, which is expected to be in the range of 10-20 MPa, and thus can be moved to the left hand side. Exact solutions for the equations above are rare and thus we use an iterative process to solve this problem. The iterative processes will begin by solving for the deflection using equation 14. The next step is to solve equation 16 by using the methods used to solve for the plate equation:

$$2E\Phi_{mn}\left(\left(\frac{n\pi}{a}\right)^2 + \left(\frac{m\pi}{b}\right)^2\right)^2\frac{ab}{4} + \iint_A\left[\frac{\partial^2 w_o}{\partial x^2}\frac{\partial^2 w_o}{\partial y^2} + \frac{\partial^2 w_o}{\partial y^2}\frac{\partial^2 w_o}{\partial x^2} - 2\frac{\partial^2 w_o}{\partial x\partial y}\frac{\partial^2 w_o}{\partial x\partial y}\right]\sin\frac{n\pi x}{a}\sin\frac{m\pi y}{b}\,dxdy = 0 \quad (17)$$

Where w_o is the current estimate for the deflection w that was obtained from the previous step. The only major task here is to solve for the definite integral as shown above. Due to the nature of the definite integral that has periodic functions with respect to x and y, many numerical integration methods can be used. The only requirement is for accurate solutions the sampling rate must be larger than the maximum spatial frequency, $N\pi/a$, as describe by the Nyquist sampling theory. An eleven point Newton-Cote integration rule seemed to be sufficient for each actuator. In Adaptive Optics this much numerical accuracy may not be necessary since spatial frequencies smaller than the actuator distance are not measured by the wavefront sensor.

The next task is to solve equation 15 with use of the newly obtained estimate for Φ. Once again the solution for a definite integral is needed and this can be done numerically as described above. Table 3 shows the steps described above along with matrix representation of the equations needed. Steps 3 and 4 should be repeated until the desired relative error is achieved.

Table 3. Nonlinear plate equations, matrix representation and useful equations.

1. Solve for initial w using equation 14: (each row represents an index m,n in equation 14). $[A][W]=[P_e]$
2. Use equation 17 to solve for Φ. $[B][\Phi]=[F(w_o)]$
3. Use equation 14 & 15 to solve for the new deflection w. $[A][W]+[\sigma D][W]=[P_e]+[G(w_o+\Phi)]$
4. Repeat 2 & 3 until the desired relative error is achieved.

$$f_{mn}(w_o) = -\iint_A\left[\frac{\partial^2 w_o}{\partial x^2}\frac{\partial^2 w_o}{\partial y^2} + \frac{\partial^2 w_o}{\partial y^2}\frac{\partial^2 w_o}{\partial x^2} - 2\frac{\partial^2 w_o}{\partial x\partial y}\frac{\partial^2 w_o}{\partial x\partial y}\right]\sin\frac{n\pi x}{a}\sin\frac{m\pi y}{b}\,dxdy$$

$$g_{mn}(w_o,\Phi) = \frac{4}{Dab\pi^4}h\left[\frac{\partial^2 w}{\partial x^2}\left(\frac{\partial^2\Phi}{\partial y^2} + \sigma_x\right) + \frac{\partial^2 w}{\partial y^2}\left(\frac{\partial^2\Phi}{\partial x^2} + \sigma_y\right) - 2\frac{\partial^2 w}{\partial x\partial y}\left(\frac{\partial^2\Phi}{\partial x\partial y} + \sigma_{xy}\right)\right]$$

$$p_{mn} = \frac{4}{Dab\pi^4}\sum_{c=1}^{R}\frac{1}{2}\frac{\varepsilon A}{(g-w_o)^2}V_c^2\sin\frac{m\pi x_c}{a}\sin\frac{n\pi y_c}{b}$$

F, G, and P are $M*N$ column vectors

$$a_{mn,ij} = \left(\left(\frac{m}{a}\right)^2 + \left(\frac{n}{b}\right)^2\right)^2\delta_{mn,ij} + \frac{4k}{Dab\pi^4}\sum_{c=1}^{R}\left[\sin\frac{i\pi x_c}{a}\sin\frac{j\pi y_c}{b}\right]\sin\frac{m\pi x_c}{a}\sin\frac{n\pi y_c}{b}$$

A is a (M*N)x(M*N) matrix (m,n is the row, i,j is the column).

3. SIMULATION RESULTS

Using the methods describe above we will simulate a 9*9 MEMS DM with a 2 µm mirror surface. The mirror layer as well as the spring layer is gold. The distance between actuators is set to 1 mm. Table 1 shows the initial design parameters for this simulation. We will start by simulating the pull-in characteristics of the MEMS DM. The center actuator will be powered while the others around it are off.

3.1 Nonlinear simulation

Fig. 3 shows the results of simulating a 9x9 MEMS DM, only the center actuator has been powered close to the pull-in voltage. The deflection *w* is measured relative to the top of the membrane and a positive value for *w* indicates a deflection towards the second conductor, i.e. pulling on the membrane from the bottom. From the figure we can estimate that the 20% influence function extends about 1 actuator (1 mm) out from the powered actuator and that most of the influence function has flattened out after a distance of 2 actuators. The center actuator pulls on the mirrors surface and the actuators around it act as pivots preventing the mirror from lifting and thus introducing a small inclination angle, ~.6 degrees. This angle must be continuous on the other side of the actuator, but the second nearest actuator introduces further resistance, which creates the local minimum between the two. From the information gathered on the influence function we can design a 2 actuator boundary for our MEMS DM which will prevent the edges of the mirror from influencing the DM pull-in characteristics. Selecting the appropriate boundary will also prevent the residual stress from deforming the mirror layer. From this we should conclude that the design of the mirror layer should resemble a hinge, little or no deflection at the edges and the angle at the edges is continuous (also called simply supported).

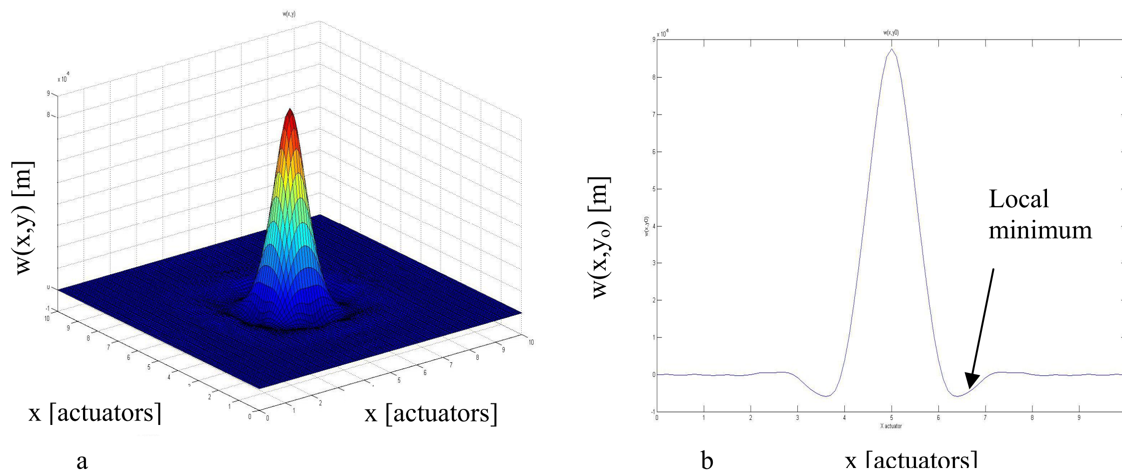

Fig. 3. 9x9 MEMS DM simulation. The x and y axis are measured in actuator spacings (i.e 1 mm change), and w is measured in meters. a) shows a 3D surface plot of the deflection. b) shows a center line cut of the plot in a. The maximum deflection is 8.6 µm.

Fig 4 shows the maximum deflection of w as the voltage is varied. As we can see the nonlinear stretching of the membrane has increased the load carrying capacity and the pull in voltage has increased. We should also note that the amount of usable gap has increased to 12µm or 40 percent of the initial gap. This is a very good result since more of the gap can be used for mechanical stroke. As a design consideration the gap should be kept at 30 µm in order to reach the desired stroke before pull-in. Fig 3 also shows the results of adding 10 and 20 GPa of tensile stress to the membrane. The pull-in voltage is further increased for both the 10 and 20 GPa curves. This is expected since we know that tensile stress makes the mirror layer stiffer. Note that compressive stress would cause the membrane to buckle thus leading to a very unstable surface. The simulations also show that the stress on the mirror surface had increase to 1% of the yield strength: at 12 µm for the case with no stress, at 10.5 µm for the case with 10 GPa, and at 10 µm for the case with 20 GPa stress. This should be taken into account since care must be taken no to surpass more than 2% percent so as not break the

membrane at any of its weakest point. The weakest points on the membrane usually manifest themselves at points where the mechanical polishing thins the mirror layer and at sharp corners.

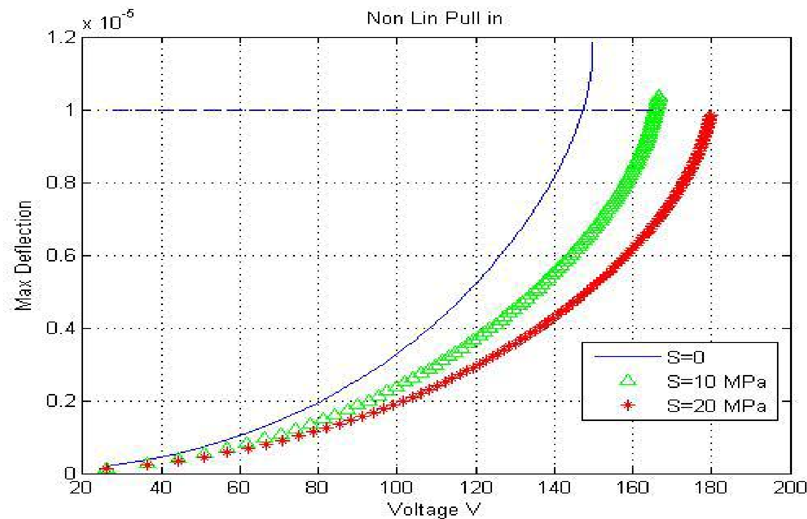

Fig. 4. Maximum deflection of a 9x9 MEMS DM with 0, 10 GPa, and 20 GPa of tensile stress.

4. CONCLUSION

This paper shows the simulations of a MEMS DM using the nonlinear electrostatic actuator equations and the nonlinear plate equation. The simulation was derived by using the Galerkin's energy method. The set of orthogonal functions, sinusoidal with period equal to the mirror size, satisfied the boundary condition for the MEMS DM design. The simulations showed a 20 percent increase in pull-in voltage as the stress increase from no stress to 20 GPa of tensile stress. From the simulation we also concluded that the points with maximum stress were at the posts and the there is an overall increase in stress at those points as the voltage increases. The simulation also showed the overall shape of the influence function which only extends about 1 actuator for a 20% drop from maximum.

ACKNOWLEDGMENT

This work was supported in part by the National Science Foundation Science and Technology Center for Adaptive Optics, managed by the University of California at Santa Cruz under cooperative agreement AST 98-76783.

REFEEENCES

1. Norbert Hubin et. al, *Adaptive Optics for Extremely Large Telescopes*, Proc. IAU Symposium, No. 232, pp. 60-85 (2005).
2. Boston Micromachines Corporation, http://www.bostonmicromachines.com/products.htm last accessed on Dec. 16 2007.
3. Iris AO, Inc., http://www.irisao.com/ last accessed on Dec. 16 2007.
4. Julia W. Evans, *Demonstrating sub-nm closed loop MEMS flattening*, Optics Express, Vol. **14**, Issue 12, pp. 5558-5570 (2006).
5. HT Micro, http://www.htmicro.com/html/technology.htm, last accessed on Dec 18 2007.
6. Bautista Fernandez and Joel Kubby, *Design, processing and materials for large-stroke actuators*, Proc. of SPIE, Vol. **6467**, p. 64670T (2007).
7. Rudolph Szilard, Theory and Analysis of Plates: Classical and Numerical Methods, Prentice Hall, New Jersey 1974.